Absence of mean-free-path effects in the current-perpendicular-to-plane magnetoresistance of magnetic multilayers

K. Eid,[1] D. Portner,[1] J. A. Borchers,[2] R. Loloee,[1] M. Al-Haj Darwish,[1] M. Tsoi,[1] R. D. Slater,[1] K. V. O'Donovan,[2] H. Kurt,[1] W. P. Pratt, Jr.,[1] and J. Bass[1]

[1]*Department of Physics and Astronomy, Center for Fundamental Materials Research, and Center for Sensor Materials, Michigan State University, East Lansing, Michigan 48824*

[2]*NIST Center for Neutron Research, National Institute of Standards and Technology, Gaithersburg, Maryland 20899*

(Received 4 September 2001; published 14 January 2002)

The series resistor and Valet-Fert models widely used to describe the current-perpendicular-to-plane (CPP) magnetoresistances of ferromagnetic/nonmagnetic (F/N) metal multilayers were recently claimed to be valid only for mean-free paths shorter than layer thicknesses; otherwise the mean-free path was claimed to be an important length scale in the CPP magnetoresistance (MR). This claim was based on observations of differences in the CPP MR's, after the samples were taken to above their saturation magnetic fields, of two different kinds of multilayers involving Co and Cu: interleaved $[\mathrm{Co}(6)/\mathrm{Cu}(20)/\mathrm{Co}(1)/\mathrm{Cu}(20)]_N$ and separated $[\mathrm{Co}(6)/\mathrm{Cu}(20)]_N[\mathrm{Co}(1)/\mathrm{Cu}(20)]_N$, with N repeats and thicknesses in nm. The maximum CPP MR's of separated samples were only about half as large as those for interleaved ones. In two short papers, we provided experimental evidence that mean-free paths are not important length scales in the CPP MR by showing that the differences in CPP MR's upon which the above claim was made did not change when the mean-free paths in the N and F layers were reduced from well above to well below their layer thicknesses. We ascribed part of the behaviors of interest to finite spin-memory loss (spin flipping) in the F and N metals, and proposed that the rest might be due to spin flips at F/N interfaces. In the present paper we (a) present further experimental evidence against mean-free-path effects, (b) provide details of the calculations we use to analyze the data, and (c) use measurements of magnetization and polarized neutron reflectivity to show that the differences in CPP MR are not due to spurious differences in magnetic structure between interleaved and separated multilayers, but only to the differences in the relative magnetic alignment of adjacent layers. Additional evidence for this last point is our observation that the CPP MR's of separated samples in their as-prepared states are as large as those of the equivalent interleaved samples after they are taken to above their saturation fields. We show that similar differences between interleaved and separated data appear also in the current-in-plane (CIP) MR's and when the Cu is replaced by Ag.

DOI: 10.1103/PhysRevB.65.054424 PACS number(s): 75.70.Cn, 73.40.−c, 75.70.Pa

I. INTRODUCTION

Understanding quantitatively giant magnetoresistance (GMR) in ferromagnetic/nonmagnetic (F/N) multilayers is important for science and technology. Based upon a wide range of data and analysis, it is widely accepted that the current-perpendicular-to-plane (CPP) magnetoresistance (MR) usually involves simpler equations than the more standard current-in-plane (CIP) MR, and thus usually gives more direct access to the fundamental physics of GMR.[1–8] The CIP MR has three scaling lengths, the mean-free path in the N metal λ_N and those for electrons with moments along $\lambda_F^{\uparrow}$ or opposite to $\lambda_F^{\downarrow}$ the F-layer magnetization. In CIP-MR equations, these lengths appear in exponential functions as ratios with the layer thicknesses[2]—e.g., $\exp(-t_N/\lambda_N)$. In contrast, according to the theory of Valet and Fert (VF),[5] in the CPP MR the scaling lengths are the spin-diffusion lengths (spin-flip lengths) in the N and F metals, l_{sf}^N and l_{sf}^F. Since scattering events with spin flips are usually only a fraction of all scattering events, l_{sf} is normally expected to be longer than λ. When these lengths are longer than their respective layer thicknesses $l_{sf}^N \gg t_N$, and $l_{sf}^F \gg t_F$, they drop out of the CPP MR, yielding a simple two-current series resistor (2CSR) model. In that model, the only lengths are the layer thicknesses t_N and t_F, which appear only algebraically. This dependence only on t_N and t_F was tested early on[1,9] by comparing data in a particular form for samples with the same F metal Co but different N metals [Cu vs Cu(4%Ge), or Ag vs Ag(4%Sn)]. This alloying of Cu or Ag changed λ_N by up to a factor of 20, but left l_{sf}^N and l_{sf}^F long enough so that the 2CSR model was expected to apply. Agreement of these data[1,6,9] with the predictions of the 2CSR model implied that the model represented a good approximation to the physics underlying the CPP MR of these metals, and seemed to show that λ_N, $\lambda_F^{\uparrow}$, and $\lambda_F^{\downarrow}$ are not scaling lengths of the CPP MR.

Recently, however, the applicability of the 2CSR and VF models was challenged,[10] based upon a combination of theoretical analysis with observation of qualitatively different MR's for two different geometries of samples composed of Co layers with thicknesses $t_{Co}=6$ nm or 1 nm alternated with Cu layers thick enough ($t_{Cu}=20$ nm) to eliminate exchange coupling between the Co layers. The geometries are called ''interleaved'' $[\mathrm{Co}(6)/\mathrm{Cu}(20)/\mathrm{Co}(1)/\mathrm{Cu}(20)]_N$ or ''separated'' $[\mathrm{Co}(6)/\mathrm{Cu}(20)]_N[\mathrm{Co}(1)/\mathrm{Cu}(20)]_N$, where italic N indicates the number of repeats. Because the saturation magnetic field H_s of Co layers of macroscopic area increases with decreasing t_{Co}, the use of two very different values of t_{Co} should allow for antiparallel (AP) alignment of

the magnetic moments of thin and thick Co layers over a limited field range. Analysis of experimental data should thus be straightforward. Because the only lengths in the series resistor CPP-MR equations are t_{Co} and t_{Cu}, those equations predict that the MR's of separated and interleaved samples should be identical.

The filled circles and solid curves in Fig. 1 (obtained after the samples were first taken to saturation) show that we confirm the differences in $A\Delta R(H)=AR(H)-AR(\mathrm{P})$ reported[10] for interleaved and separated samples with $t_{Co}=6$ nm and 1 nm and $t_{Cu}=20$ nm for $N=4$, 6, and 8. A is the sample area through which the CPP current flows, $R(H)$ is the CPP resistance at H, and P indicates the high field limit where the Co layer magnetizations are all aligned parallel (P) to each other. For interleaved samples, the AP states occur at the maxima of $AR(H)$. For separated samples, we must distinguish between two different AP states, the first (like that of interleaved samples) where alternate-layer magnetizations are aligned AP, and the second where the magnetizations of thick and thin layers are aligned AP. The solid symbols in Fig. 1 show that the AR's for the second state (''plateaus'' for $H\sim 250$ Oe, see Sec. IV A) differ from those for the AP state in the interleaved samples (peaks at $H\sim 250$ Oe). In contrast, as we will discuss in detail in Sec. IV A, the open symbols and dashed curves for the separated samples (measured while the samples were first taken to saturation) show that the first state (located at $H=0$ for this condition—see Sec. IV A) gives AR roughly the same as $AR(\mathrm{AP})$ for the interleaved state and, more importantly, closely similar values of $A\Delta R=AR(\mathrm{AP})-AR(\mathrm{P})$. We can, thus, make the experimental quantities $AR(\mathrm{AP})$ and $A\Delta R$ almost unique by limiting the use of the symbol $AR(\mathrm{AP})$ to the case where the magnetizations of *adjacent layers* are aligned AP. For a separated sample in the second state, we will not use the symbol $AR(\mathrm{AP})$, but refer only to $AR(H)$ for the AP state. These definitions give CPP $\mathrm{MR}(H)=A\Delta R(H)/AR(\mathrm{P})$, with maximum CPP $\mathrm{MR}=A\Delta R/AR(\mathrm{P})$. In all figures showing $AR(H)$, the scale divisions for interleaved and separated samples are the same, allowing direct visual comparison of their forms and magnitudes.

The solid curves of $AR(H)$ for the interleaved samples consist of a single broad peak, symmetric about $H=0$. This is the qualitative behavior expected from the 2CSR model as the magnetic order of the layer magnetizations in the sample reorients from P at high H to AP for values of H between the saturation fields of the $t_{Co}=6$ and 1 nm layers. The solid curves of $AR(H)$ for the separated samples, in contrast, are more complex, with maximum values of $A\Delta R(H)$ only about half those for the interleaved samples. For the smallest N shown ($N=4$), there is a sharp peak followed by a broad plateau. For the largest ($N=8$), there are two separate peaks, corresponding almost to the sum of separate contributions from the 6 and 1 nm Co layers.

Differences in $A\Delta R(H)$ for interleaved and separated samples similar to those in the solid curves in Fig. 1 were reported previously in samples of Co and Permalloy (Py $=\mathrm{Ni}_{1-x}\mathrm{Fe}_x$ with $x\sim 0.2$) with Ag,[11] or Co and Fe with Cu.[12] In the first case, the difference was attributed to short l_{sf}^{Py}. In the second, short l_{sf}^{Fe} was taken as part of the explanation, but possible spin-memory loss at F/N interfaces was also proposed. In contrast, the authors of Ref. 10 argued that l_{sf}^{Co} and l_{sf}^{Cu} were too long for spin-memory loss within the Co and Cu to be important. They argued that the 2CSR and VF models break down when the mean-free paths become larger than the layer thicknesses—that ''mean-free-path effects'' then appear. Their argument is not simply one of changing magnitude of AR as the resistivities ρ_F and ρ_N of the F and N layers change. [We will see in Sec. III that ρ_F and ρ_N appear explicitly in the 2CSR and VF models, and that these models can approximately account for the observed changes in magnitude of $AR(H)$ due simply to changes in ρ_N and/or ρ_F.] Rather, they argued that ratios t/λ appear explicitly in equations that differ from those of both the 2CSR and VF models. If they are correct, then the differences in behavior in Fig. 1 should gradually disappear as the ratio t/λ is increased.

This claim was tested in two ways.[13,14] First, we replaced Cu by a dilute Cu(2%Ge) alloy (hereafter just CuGe) with a short mean-free path $\lambda_{CuGe}\sim 8$ nm, but a long spin-diffusion length $l_{sf}^{CuGe}\sim 130$ nm.[9,13] Such alloying should mainly reduce λ_{Cu}. As shown in Fig. 2 for samples identical to those in Fig. 1 except with Cu replaced by CuGe, increasing the ratio t_{Cu}/λ_{Cu} by up to a factor of 25 (from $\sim 1/5$ for our sputtered pure Cu to ~ 5 for the thickest sputtered CuGe layers in Fig. 3 and Ref. 13) produced no significant change from Fig. 1 in either the forms or relative magnitudes of interleaved and separated samples. Second, in addition to replacing Cu by CuGe, we also replaced[14] the 6 nm Co layers by 15 or 30 nm thick layers of Co(2%Zr) (hereafter just CoZr) and the 1 nm Co layers by 30 nm thick layers of Py, both of which have mean-free paths much shorter than these layer thicknesses. If anything, the differences (Fig. 4 and Ref. 14) increased. Such behavior is opposite to that expected from mean-free-path effects, but is expected if the CPP MR is dominated by short spin-diffusion lengths in CoZr and Py.

Our data, thus, strongly suggest that the ratio t/λ is not driving the differences in behavior shown in Fig. 1. The question then remains, what is driving those differences? In Secs. III and IV, we show that the differences can be partly attributed to spin-memory loss in the bulk metals, and the rest can be reasonably well fit by spin-memory loss at Co/Cu interfaces.[13]

The rest of this paper is organized as follows. In Sec. II, we briefly describe sample preparation, sample characterization, and our experimental procedures. In Sec. III, we first review theoretical issues and the 2CSR and VF models. We then describe the VF-based numerical calculations that we use to analyze our data. Finally, we consider what effects would be produced by spin-memory loss at F/N interfaces. In Sec. IV we present additional data and analysis. Crucial to any simple interpretation of the data is the requirement that the magnetic structures in interleaved and separated samples not differ in spurious ways. We use magnetization M, CPP MR, and polarized neutron reflectivity measurements to argue that they do not. Section V contains a summary and conclusions.

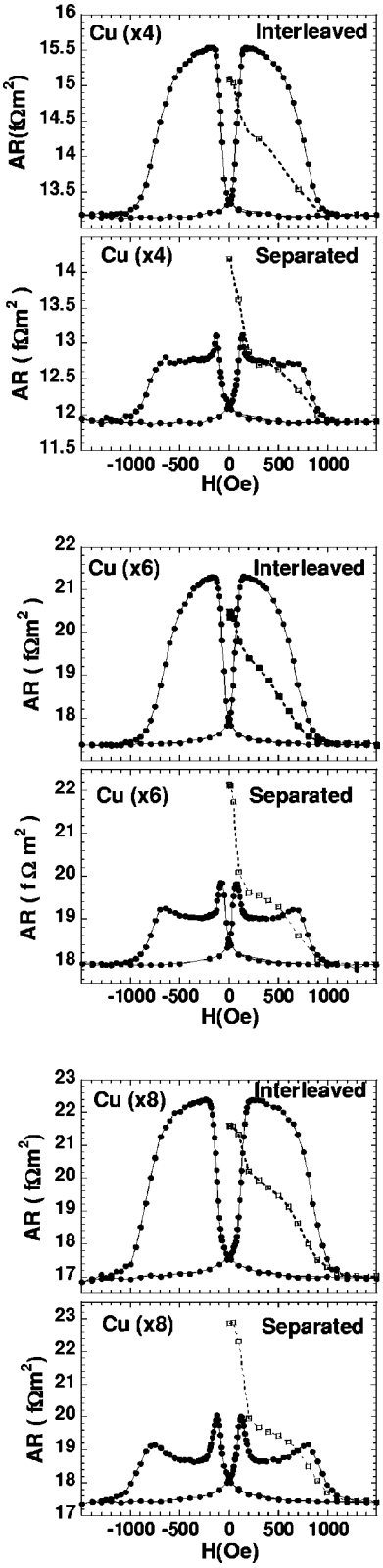

FIG. 1. $AR(H)$ vs H at 4.2 K for interleaved (top of each pair) and separated (bottom of each pair) multilayers of Co/Cu with $N=4$, 6, and 8. The scale units for each coupled pair are identical. The open squares and dashed curves show how $AR(H)$ varied when first taken from the as-prepared state to the saturated state. The filled circles and solid curves show how it varied after having been taken to saturation.

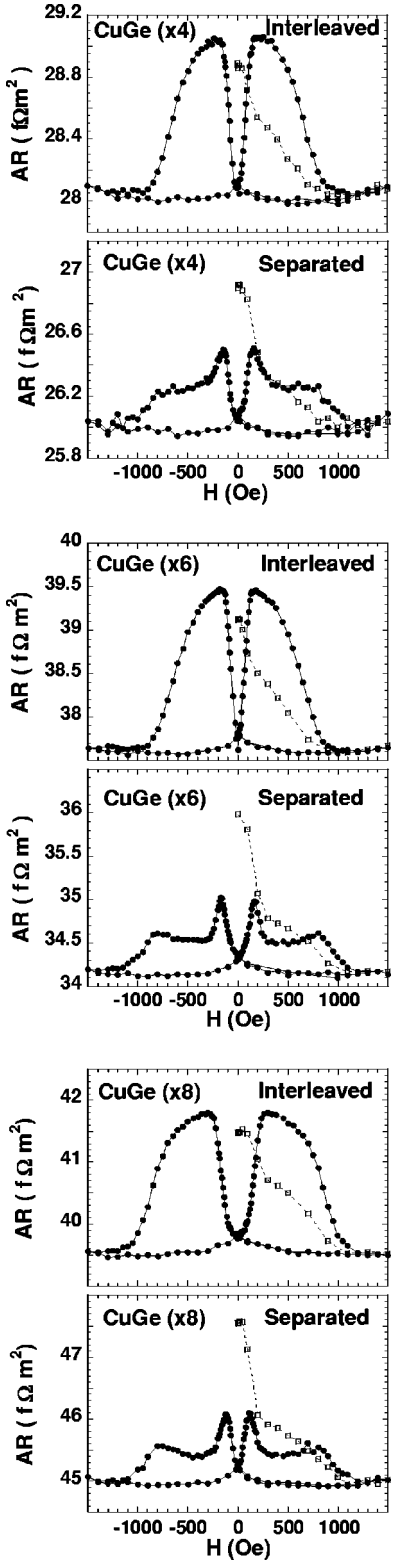

FIG. 2. $AR(H)$ vs H at 4.2 K for interleaved (top of each pair) and separated (bottom of each pair) multilayers of Co/CuGe with $N=4$, 6 and 8. The scale units for each coupled pair are identical. The symbols and curves have the same meanings as in Fig. 1.

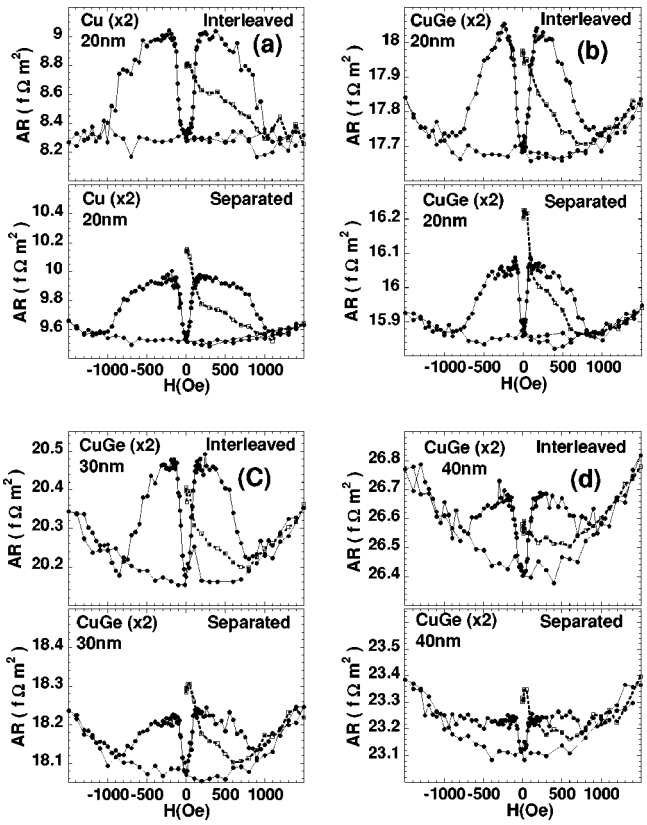

FIG. 3. $AR(H)$ vs H at 4.2 K for interleaved (top) and separated (bottom) samples with $N=2$. The samples with Cu have $t_{Cu}=20$ nm. The samples with CuGe have $t_{CuGe}=20$, 30, and 40 nm. The symbols and curves have the same meanings as in Fig. 1.

II. SAMPLES AND MEASURING TECHNIQUES AND PROCEDURES

The shapes of our samples, the use of superconducting Nb leads to ensure uniform current, and the details of our sputtering system and techniques, and general sputtering rates, are all described elsewhere.[7] We note here only that the samples were sputtered in a chamber with masking capability, so that the entire sample was sputtered *in-situ*. Each sample consisted of an ~1.1 mm wide, 250 nm thick Nb bottom strip, a wider portion of the sample composed of a 20 nm Cu (or CuGe) second layer and then the multilayer of interest, and finally a second ~1.1 mm wide, 250 nm thick Nb top cross strip, oriented perpendicular to the first one. The area through which the CPP current flows is thus $A \sim 1.2$ mm^2.

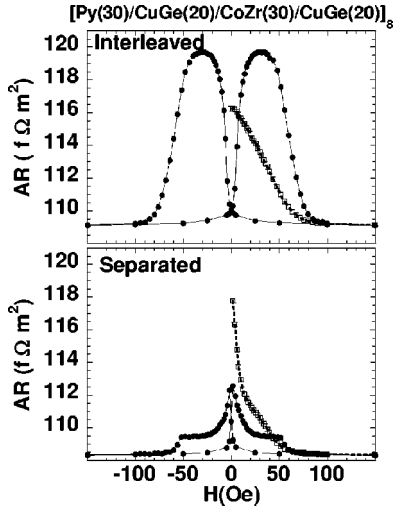

FIG. 4. $AR(H)$ vs H at 4.2 K for an interleaved (top) and a separated (bottom) multilayer composed of CoZr, CuGe, and Py. The symbols and curves have the same meanings as in Fig. 1.

The Cu(2%Ge) layers were sputtered at a rate of ~1 nm/s from an alloy target prepared by induction melting. Van der Pauw resistivity measurements at 4.2 K of six different sputtered films gave $\rho=80\pm5$ nΩm, corresponding to 2%Ge and $\lambda=8\pm1$ nm.[15] Sputtered films analyzed by electron energy-dispersive scattering (EDS) gave a similar value ~2.5%Ge. The Py and CoZr alloys were sputtered at ~0.5 nm/s from targets made for other studies. Their parameters will be given in Sec. III.

To avoid the strong diamagnetism of a superconductor, magnetizations M were measured at 12 K, above the superconducting transition temperature (~9 K) of our sputtered Nb. M was measured both on entire samples (allowing comparison of absolute magnitudes for interleaved and separated samples) and also on the $A\sim1.2$ mm^2 "central pieces" through which the CPP current flows. Similar results were obtained with both geometries.

The magnetic structures in these samples were also characterized using polarized neutron reflectivity (PNR), which is sensitive to the interaction between the sample's magnetization and the magnetic moment of the neutron. PNR measurements were performed at the NIST Center for Neutron Research on multilayers prepared in the same way as those for the CPP-MR studies, except that the samples were squares, 1.27 cm on a side, and sputtered directly onto the Si substrates instead of onto Nb. All PNR measurements were made at 17–18 K after cooling in zero field in a closed-cycle refrigerator. An electromagnet provided a maximum field of 2 kOe. Using neutrons of wavelength $\lambda=0.475$ nm on the NG-1 reflectometer, we measured the non-spin-flip (NSF) reflectivities R^{++} and R^{--}, as well as the spin-flip (SF) reflectivities R^{+-} and R^{-+}. (The + and − signs in the superscripts describe the polarization state of the incident and scattered neutron spins. These spins are aligned either parallel + or antiparallel − to the applied field.) The selection and detection of the neutron spin state is described elsewhere.[16] The NSF reflectivities sense the chemical structure of the multilayer, and the splitting between R^{++} and R^{--} is sensitive to the component of the in-plane magnetization parallel to the applied field. The SF reflectivities are primarily sensitive to the projection of the in-plane magnetization that is perpendicular to the applied field. We measured both the specular and diffuse (i.e., off-specular) reflectivity as a function of the wave vector $Q_z=4\pi\sin\theta/\lambda$, where θ is the angle of the incident and scattered neutrons relative to the sample surface. We obtained the diffuse data by offsetting the sample normal by 0.1° relative to the specular scattering condition and then scanning Q_z. These diffuse measurements provide general information about the growth-axis

correlations among in-plane ferromagnetic domains with dimensions smaller than 100 μm (Refs. 17–19) and were also subtracted from the total reflectivity to give the specular reflectivity. After next correcting the specular data for the efficiencies of the polarizing elements (which range from 92–100 %), fits to the data yield a profile of the vector magnetization as a function of depth for regions of the multilayer with ferromagnetic domains larger than approximately 100 μm within the sample plane.[16–19]

III. THEORY

A. Free-electron models

When electronic transport occurs via diffusion, and spin flipping is rare, it is accepted that free electron analysis of the CPP MR yields a simple 2CSR model for AR(AP) and AR(P).[1,4,5,10] In this model, the total AR of the sample in each state is given by the parallel combination of the series sum for each current channel (i.e., electron moments along or opposite to the direction of positive H) of resistivities times layer thicknesses $\rho_{Cu}t_{Cu}$, $\rho^{\uparrow}_{Co}t_{Co}$, and $\rho^{\downarrow}_{Co}t_{Co}$ plus areas times interface resistances $AR^{\uparrow}_{Co/Cu}$ and $AR^{\downarrow}_{Co/Cu}$. We also define scattering anisotropy parameters[1,5] $\beta=(\rho^{\downarrow}_{Co}-\rho^{\uparrow}_{Co})/(\rho^{\downarrow}_{Co}+\rho^{\uparrow}_{Co})$ and $\gamma=(AR^{\downarrow}_{Co/Cu}-AR^{\uparrow}_{Co/Cu})/(AR^{\downarrow}_{Co/Cu}+AR^{\uparrow}_{Co/Cu})$. We focus upon AR(AP) and $A\Delta R$. For both interleaved and separated samples with $2N$ layers of Cu with $t_{Cu}=20$ nm and N layers each of Co with $t_{Co}=6$ nm or 1 nm, the series resistor model gives the same expressions:

$$AR(\mathrm{AP})=2AR_{Nb/Co}+2N\rho_{Cu}\times(20\ \mathrm{nm})+N\rho^{*}_{Co}\times(6\ \mathrm{nm})+N\rho^{*}_{Co}\times(1\ \mathrm{nm})+4NAR^{*}_{Co/Cu} \quad (1)$$

and

$$A\Delta R=4N^{2}[\beta_{Co}\rho^{*}_{Co}\times(6\ \mathrm{nm})+2\gamma_{Co/Cu}AR^{*}_{Co/Cu}]\times[\beta_{Co}\rho^{*}_{Co}\times(1\ \mathrm{nm})+2\gamma_{Co/Cu}AR^{*}_{Co/Cu}]/AR(\mathrm{AP}), \quad (2)$$

where, for simplicity in writing the equations here, we have neglected differences between N and $N-1$ (such differences are, of course, included in actual calculations). $2AR_{Nb/Co}=(6\pm1)$ fΩm^2 is twice the Nb/Co interfacial specific resistance, ρ_{Cu} is the independently measured Cu resistivity, $\rho^{*}_{Co}=(\rho^{\uparrow}_{Co}+\rho^{\downarrow}_{Co})/4=\rho_{Co}/(1-\beta^2)$ is the average resistivity of Co in the AP state, and $AR^{*}_{Co/Cu}=(AR^{\uparrow}_{Co/Cu}+AR^{\downarrow}_{Co/Cu})/4$ is the similarly averaged Co/Cu interface specific resistance.

For our present purposes, the most important features of Eqs. (1) and (2) are the following. (1) The only lengths in Eqs. (1) and (2) are the layer thicknesses t_F and t_N. (2) If the Cu is doped with a dilute concentration of an impurity, such as Ge, that increases ρ_{Cu}, but leaves l_{sf} long and does not significantly change β_{Co}, $\gamma_{Co/Cu}$, or $AR^{*}_{Co/Cu}$, then AR(AP) should increase only by the increase in $\rho_{CuGe}t_{CuGe}$ over $\rho_{Cu}t_{Cu}$, and $A\Delta R$ should decrease only because of this increase in AR(AP) in the denominator of Eq. (2). Quantitatively, Eq. (2) then predicts that replacing Cu by CuGe should reduce $A\Delta R$ by the ratio $[AR(\mathrm{AP})_{Cu}/AR(\mathrm{AP})_{CuGe}]$. Comparing Figs. 1 and 2 shows that this simple prediction gives a decent first approximation to the relative behaviors therein.

In contrast, when spin flipping occurs, VF theory gives more complex equations, where the ratios t_F/l^{F}_{sf} and t_N/l^{N}_{sf} appear as arguments of exponentials.[5] Except in the simplest cases, the VF equations must be solved numerically. The 2CSR model is the limit of VF theory when these ratios are small. For this reason, we believe that an argument made in Ref. 10 is incorrect. Specifically, the authors[10] claimed that the 2CSR model is some kind of a ''local model,'' and that a model involving contributions to AR only from neighboring F layer is ''nonlocal.'' Instead, the 2CSR model is the extreme limit of a ''nonlocal'' model, in which AR is determined by the relative orientations of all of the F layers in the sample. We will see in Sec. III C that the so-called ''nonlocal'' model is equivalent to the extreme opposite VF limit where t_F/l^{F}_{sf} is very large. The model designated ''nonlocal'' is, in fact, the most ''local'' model that gives a CPP MR.

B. Possible real Fermi surface effects

So far, we have assumed free-electron metals. But it now seems that, absent spin-flip scattering, CPP-MR data should conform to the form of the 2CSR model even for metals with real band structures, so long as the transport is completely incoherent.[20] In this limit, the remaining issue seems to be whether the interfacial specific resistance $AR^{*}_{F/N}$ can be explained solely on the basis of differences in band structure, or whether interfacial mixing and roughness are also important. Calculations that allow some coherence, limited by either bulk disorder[10] or interfacial intermixing,[21] show deviations from the 2CSR model. In Ref. 10, such deviations in the presence of bulk disorder, but with mean-free paths longer than the layer thicknesses, were called ''mean-free-path'' effects and were proposed to explain the data of Fig. 1. The experimental question before us is when such effects are significant.

As noted in the Introduction, a wide range of CPP-MR data[1–8] involving F=Co and N=Cu or Ag are well described by the 2CSR model. Also, where differences in form of the CPP-MR data for interleaved and separated samples of Co/Ag/Py/Ag (Ref. 11) and Co/Cu/Fe/Cu multilayers[12] were seen earlier, they could plausibly be attributed to finite spin-diffusion lengths in the Py and Fe. While the authors of Ref. 10 did not formally challenge this latter interpretation, one subsequently[22] raised the possibility that the differences seen[11,12] might also arise from mean-free-path effects instead of finite spin-diffusion lengths. To test this possibility, we replaced the 6 and 1 nm thick layers of Co in interleaved multilayers with much thicker layers of alloys that have much higher resistivities and thus much shorter mean-free paths (see Fig. 4). Based on prior studies, we chose 30 nm thick layers of Py (a well studied ''low H_s'' alloy) to replace the 1 nm thick Co layers, and 15 and 30 nm thick layers of CoZr (an alloy with a large resistivity per atomic percent impurity[15]) to replace the 6 nm thick Co layers. Independent

measurements of the resistivities of our sputtered Py and CoZr give $\rho_{Py} \approx 120$ nΩm (Ref. 23) and $\rho_{CoZr} \approx 200$ nΩm (Ref. 24).

C. VF theory with interfacial spin-memory loss

In Sec. III A we wrote down the 2CSR equations that apply equally well to both interleaved and separated samples. In VF theory, in contrast, the equations for interleaved and separated samples differ. Qualitatively, if spin-memory loss occurs in the F or N metals, or at F/N interfaces, but is not too strong, then $A\Delta R$ for interleaved samples is only modestly affected by such loss, but $A\Delta R$ for separated ones is substantially reduced due to ''GMR decoupling'' of different layers that are far apart. The VF equations are so complicated that we must solve them numerically. We briefly describe our procedure and some results.

VF theory treats spin-polarized transport through a multilayer in terms of spin dependent, spatially varying, electrochemical potentials and currents. Each layer is characterized by two lengths, the layer thickness and the layer spin diffusion length l_{sf}. At the layer boundaries, the chemical potentials and currents are matched, taking account of interfacial specific resistances where needed but neglecting any interfacial spin memory loss. Fert and Lee[25] included interfacial spin-memory loss by defining a ''spin-flip'' interface resistance. We use an alternative procedure for F/N interfacial spin flips that builds upon our treatment of spin-memory loss at interfaces between nonmagnetic metals.[26] We represent the F/N interface by an additional ''layer'' (I), taken to be a homogeneous slab of thickness t_I, resistivity ρ_I, ''bulk'' scattering anisotropy β_I (chosen equal to the interfacial $\gamma_{F/N}$) and spin diffusion length l^I_{sf}, subject to the constraint $AR^*_{F/N} = \rho_I t_I$. VF theory then involves matching electrochemical potentials and currents at the boundaries of this I layer with the F and N metals. Such matching depends only on two parameters, the interfacial spin-memory-loss parameter $\delta_I = t_I / l^I_{sf}$, and the product $\rho_I l^I_{sf}$. However, the constraint $AR^*_{F/N} = \rho_I t_I$ lets us write $\rho_I l^I_{sf} = AR^*_{F/N}/\delta_I$, leaving only a single independent parameter δ_I to control the process, independent of any particular choice of t_I—i.e., t_I turns out to be arbitrary.

We have written programs to solve the VF equations for interleaved and separated samples up to $N=8$ (equivalent to a standard $[F/N]_N$ multilayer up to $N=16$). As an example of a solution, we show in Fig. 5 the calculated dependences of $A\Delta R$ upon δ_I for interleaved and separated Co/Cu samples with $N=6$, taking the Co and Cu parameters in Ref. 27 and assuming, for simplicity, $l^{Co}_{sf} = l^{Cu}_{sf} = \infty$. The only unknown in the problem is then δ_I. The solid curves include the Nb/Co interface resistance $AR_{Nb/Co} = 3$ fΩm^2, at each end of the sample. For the interleaved sample, $A\Delta R$ passes through a weak maximum with increasing δ_I. Over the range from $\delta_I = 0$ to $\delta_I = 1$, $A\Delta R$ varies by little more than 10%. In contrast, for the separated sample, $A\Delta R$ decreases monotonically and rapidly; by $\delta_I = 1$ it has dropped by $\sim$75%. To clarify the source of the weak maximum in Fig. 5, we display as dashed curves in Fig. 5 the same calculation, but now taking $AR_{Nb/Co} = 0$; i.e., neglecting any contact resistance. For $\delta_I = 0$, the larger $A\Delta R$ for the interleaved and separated samples follows from Eq. (2) simply by setting $AR_{Nb/Co} = 0$ in the denominator AR(AP)—see Eq. (1). Both dashed curves now decrease monotonically with increasing δ_I (increasing interfacial spin-memory loss), and join nicely onto the solid curves for large δ_I. By large δ_I, the two Co/Nb interface resistances have dropped out of the problem—in this limit, $AR_{Nb/Co}$ can be set to zero. The initial rise in $A\Delta R$ in the solid curve for the interleaved sample is a consequence of $AR_{Nb/Co}$ gradually dropping out of the denominator of Eq. (2) as δ_I increases. This rise is an example of a counterintuitive behavior of CPP transport in the presence of a large contact resistance—increasing spin-memory loss can initially cause the CPP MR to *increase*.[28]

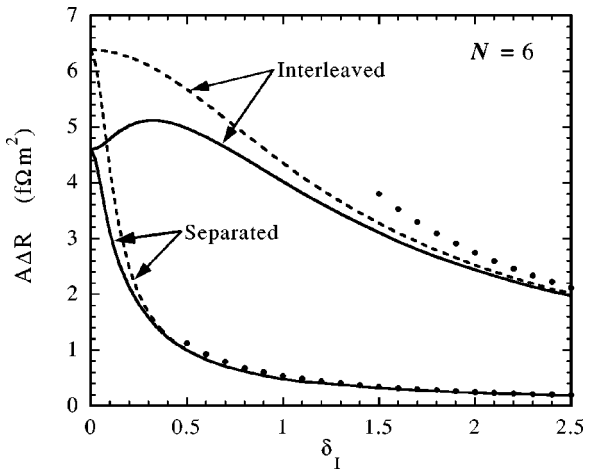

FIG. 5. Calculated values of $A\Delta R$ vs δ_I for interleaved and separated multilayers with $N=6$. The solid curves include the Co/Nb contacts; the dashed curves are the same calculations but without those contacts. The filled circles correspond to Eq. (3) with $n=11$ for the interleaved case and $n=1$ for the separated one.

In the limit $\delta_I \gg 1$, the samples reduce to a linear combination of units consisting of the Cu interlayers bounded by two thin slices of Co/Cu interfaces (of thickness l^I_{sf}). $A\Delta R$ can then be described by Eq. (3), which is a simple extension of Eq. (2) to this limit:

$$A\Delta R = \frac{4n(\beta_I \rho^*_I l^I_{sf})^2}{2\rho^*_I l^I_{sf} + \rho_{Cu} t_{Cu}}, \tag{3}$$

where for separated samples $n=1$ and for interleaved samples $n=2N-1$. As expected, the solutions of Eq. (3) (solid circles in Fig. 5) agree with the numerical solutions (curves) in the large δ_I limit. These two limits of Eq. (3) are equivalent to the results of the ''nonlocal'' model.[10] $A\Delta R$ for the interleaved samples is the sum of contributions from $2N-1$ sandwiches composed of two Co/Cu thin slices on opposite sides of each Cu layer, because the magnetizations reverse from each Co layer to the next. Importantly, as shown by the open squares and dotted curves in Figs. 1 and 2, this same value of $A\Delta R$ is seen in the as-prepared state of separated samples, and almost the same value is seen in the as-prepared state of interleaved ones. We will see in Sec. IV A that the magnetizations of adjacent layers also reverse

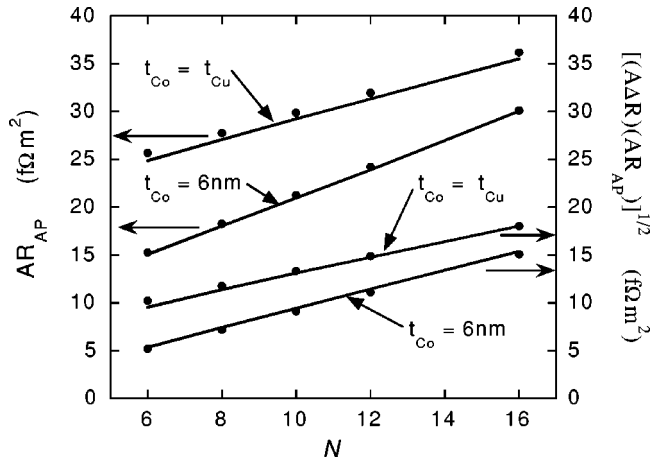

FIG. 6. Calculated values of $AR(\mathrm{AP})$ (left scale) and $\sqrt{AR(\mathrm{AP})[A\Delta R]}$ (right scale) for multilayers with total thickness $=360$ nm and either fixed $t_{\mathrm{Co}}=6$ nm or $t_{\mathrm{Co}}=t_{\mathrm{Cu}}$. Filled circles are for the 2CSR model. Solid curves are VF calculations with $l_{\mathrm{sf}}^{\mathrm{Cu}}=500$ nm, $l_{\mathrm{sf}}^{\mathrm{Co}}=60$ nm, and $\delta_I=0.25$.

from Co layer to Co layer in the as-prepared state of the separated samples and approximately also in the as-prepared state of the interleaved ones. In contrast, after the separated samples have been taken to saturation (solid symbols in Figs. 1 and 2), the magnetizations of adjacent Co layers at the intermediate field corresponding to the AP state are all parallel to each other, except at the boundary between the two different Co thicknesses. $A\Delta R$ then contains a contribution from only the one pair of Co layers for which the adjacent layer magnetizations are opposite to each other [i.e., now $n=1$ in Eq. (3)].

We now consider what effect finite interfacial spin-memory loss with $\delta_I=0.25$ would have on the Co/Cu parameters that were previously derived assuming no spin-memory loss.[6,27] Those parameters were derived using $[\mathrm{F/N}]_N$ multilayers in which all of the F and N layers were identical, i.e., samples effectively ''interleaved.'' The solid or dashed curves for interleaved samples in Fig. 5 show that $A\Delta R$ is not sensitive to the presence of δ_I, until δ_I becomes larger than about 1. More generally, a nonzero $\delta_I \leqslant 0.25$ makes little change in the linear variations with the thicknesses t_{F} and t_{N} of the quantities $AR(\mathrm{AP})$ and $\sqrt{AR(\mathrm{AP})[A\Delta R]}$ used to determine 2CSR model parameters for multilayers of the form $[\mathrm{Co/Cu}]_N$.[6,7] To show this behavior quantitatively, Fig. 6 uses the parameters for Co and Cu given in Ref. 27 to calculate $AR(\mathrm{AP})$ and $\sqrt{AR(\mathrm{AP})[A\Delta R]}$ for fixed $t_{\mathrm{Co}}=6$ nm and for $t_{\mathrm{Co}}=t_{\mathrm{Cu}}$ as functions of N. The filled circles are calculations with the 2CSR model assuming no spin-memory loss anywhere. The solid curves are the VF model including spin-memory loss both in the bulk Co and Cu and at the Co/Cu interfaces $l_{\mathrm{sf}}^{\mathrm{Cu}}=500$ nm, $l_{\mathrm{sf}}^{\mathrm{Co}}=60$ nm, and $\delta_I=0.25$. The differences between the filled circles and solid lines are small, and the forms of the two sets of data are very similar. Recalculating the solid curves assuming, instead, $l_{\mathrm{sf}}^{\mathrm{Co}}=l_{\mathrm{sf}}^{\mathrm{Cu}}=\infty$ makes almost no change. A similar analysis for an infinite multilayer also produces little change. We conclude that adding interfacial spin flipping with $\delta_I \leqslant 0.25$ has little effect on the previous 2CSR model analysis of data for $[\mathrm{Co/Cu}]_N$ (Ref. 6) and $[\mathrm{Co/Ag}]_N$ (Ref. 7) multilayers with equal Co layer thicknesses, only requiring renormalization of the model parameters by amounts small enough to lie within the previously specified uncertainties.

In contrast to having little effect on both interleaved samples and simple $[\mathrm{Co/Cu}]_N$ multilayers, Fig. 5 shows that including interfacial spin flips with $\delta_I=0.25$ has a large effect on separated samples, and we will see in Sec. IV that it can also cause larger changes in Co-Cu based exchange-biased spin valves.

In previous papers,[13,14] we have referred to the value of $\delta_I=0.25$ as corresponding to 25% spin-memory loss at an F/N interface. For spin-memory loss at N1/N2 interfaces, the ratio $\delta=t/l_{\mathrm{sf}}$ appears in $A\Delta R$ as a simple exponential, $\exp(-\delta)$ and $\exp(-0.25)\approx 0.78$ corresponds to a 22% reduction in $A\Delta R$. When δ is not too large, it thus approximates the percentage spin-memory loss. In contrast, Fig. 5 illustrates that the situation for F/N interfaces is more complex—e.g., in interleaved or simple $[\mathrm{F/N}]_N$ multilayers, $\delta_I=0.25$ can produce little change in $A\Delta R$. So in the present paper we simply describe the results produced by $\delta_I=0.25$, and never refer to a consequent percentage spin-memory-loss.

IV. DATA AND ANALYSIS

We first consider whether the differences in Figs. 1 and 2 could arise from unwanted differences in the magnetic structures of interleaved and separated samples. We conclude that any such differences are too small to be important. We then examine differences in $AR(H)$ between interleaved and separated multilayers with various constituents and propose an interpretation of the results obtained.

A. Magnetic order

We looked for differences in magnetic order between interleaved and separated samples in three ways. (1) By direct comparison of M for interleaved and separated samples. (2) By comparing how $AR(H)$ varies for both kinds of samples when they are first taken from their as-prepared state to their saturated state and thereafter. (3) By scattering polarized neutrons from interleaved and separated samples.

1. Comparison of M for interleaved and separated samples

Figure 7 compares the values of M for whole interleaved and separated samples with both Cu and CuGe nonmagnetic metals. In both cases, the two Ms are nearly the same. Importantly, the fields at which the AP states occur are the same to within our measuring uncertainties. Figure 8 shows similar behaviors for pieces of samples involving just the areas through which CPP current flowed. In both figures, the ratios of changes in magnetization as thick and thin layers flip are about the expected 6 to 1. The peaks in $AR(H)$ for the separated samples in Figs. 1 and 2 after saturation occur about where the average layer magnetizations pass through zero for the thick layers ($\sim$100 Oe) and the thin layers ($\sim$725 Oe), respectively. Figure 8 contains the variations when the samples were first taken from their as-prepared states to

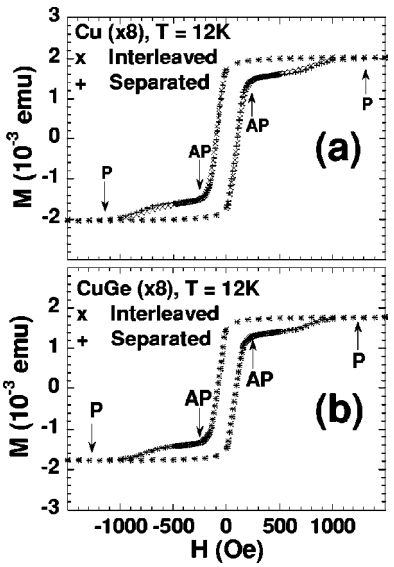

FIG. 7. M vs H at 12 K for interleaved ($\times$) and separated ($+$) samples with Cu (a) and CuGe (b) with $N=8$ for $t_{\mathrm{Cu}}=t_{\mathrm{CuGe}}=20$ nm. P and AP states are indicated.

above H_s, in addition to those when they were cycled to below $-H_s$ and back to above $+H_s$. In the as-prepared states, both magnetizations in Fig. 8 are close to zero. As H is increased from zero, M initially increases rapidly up to $H\sim 200$ Oe, then more slowly to above H_s. Both changes are only about half as large as those over the same field range after the samples have been taken to above H_s. These differences in magnetization changes before and after saturation mean that the magnetic structures of the samples differ before and after the samples are taken above H_s. To help understand the nature of this difference, we examine the related changes in $AR(H)$ before and after reaching saturation.

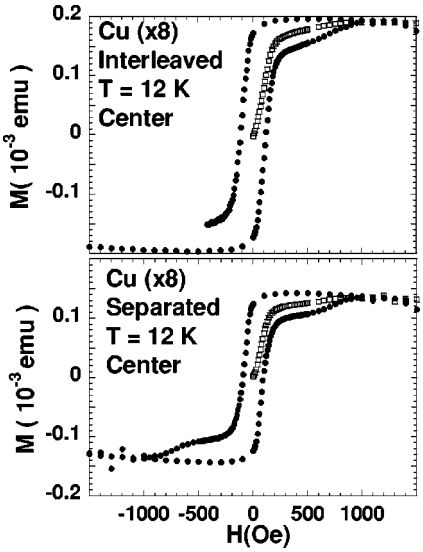

FIG. 8. M vs H at 12 K for center-cut pieces of Cu interleaved (top) and separated (lower) samples including both data from the as-prepared state to saturation and then from positive saturation to negative saturation and back again.

2. $A\Delta R(H)$ before and after saturation

Figures 1 and 2 show that the differences between $A\Delta R(H)$ for interleaved and separated multilayers are the same whether the samples contain Cu or CuGe. Once the samples have been taken to saturation, these differences are large. In contrast, when the samples are first taken from their as-prepared states to saturation, the differences in $A\Delta R(H)$ are much smaller. If we define $A\Delta R(0)=AR$ (as prepared) $-AR(\mathrm{P})$ for both interleaved and separated samples, and $A\Delta R(\mathrm{peak})=AR(\mathrm{peak})-AR(\mathrm{P})$ for interleaved samples, then we find that $A\Delta R(0)$ for separated samples is essentially the same as $A\Delta R(\mathrm{peak})$ for interleaved ones, and that $A\Delta R(0)$ for interleaved samples is about 85% of $A\Delta R(\mathrm{peak})$ for interleaved ones. Because of the differences in H_s for 1 and 6 nm thick layers of Co, we expect the magnetizations of adjacent layers in interleaved samples to be oriented nearly AP at the ''peak'' of $AR(H)$ after the samples have been taken to saturation. For these samples we thus expect $A\Delta R(\mathrm{peak})\approx A\Delta R$. Figures 1 and 2 then show that separated samples for both Cu and CuGe also have $A\Delta R(0)\approx A\Delta R$, simultaneously arguing that adjacent layers in the as-prepared states of separated samples are also ordered AP, and that $A\Delta R$ is experimentally well defined, independent of whether the thicknesses of adjacent layers are the same or different. In contrast, for interleaved samples $A\Delta R(0)\approx 0.85A\Delta R$, indicating that, in the as-prepared state, adjacent layers are not fully AP ordered.

We interpret these AR results as follows. As just noted, the close agreement between $A\Delta R(\mathrm{peak})\approx A\Delta R$ for interleaved samples and $A\Delta R(0)$ for separated ones shows that both the peak states of interleaved samples, and the as-prepared states of separated samples, are very close to the ideal AP state with magnetizations of adjacent Co layers reversed. The slightly smaller values of $A\Delta R(0)$ for the interleaved samples indicate that their magnetic orders deviate slightly from such AP states, a discrepancy we discuss below. For the interleaved samples, oppositely directed magnetizations for thick and thin layers in the as-prepared and peak states would lead to $M\neq 0$ if the layers were single domain. However, from our observations that $M(H_{\mathrm{initial}}=0)\approx 0$ (Fig. 8), as well as evidence of micron-sized domains in other studies,[18] we argue that the as-prepared states of both interleaved and separated samples consist mostly of micron-sized AP ordered domains that extend from the top to the bottom of the sample, but with the magnetizations of either the thicker or thinner Co layers oriented randomly ''positive or negative'' in the layer planes. As discussed in Ref. 18, such ordering is probably due to the fringe fields from the ends of magnetic domains. To simplify, if the bottom Co layer consists of small magnetic domains pointing only in opposite directions, such as those shown on the left sides of the figures for interleaved and separated samples in Fig. 9, then the fringe fields from these domains will act on the newly growing Co layer above to orient its domains antiparallel to those in the bottom layer. If the layer thicknesses are all the same, this process could, in principle, yield the ''ideal'' as-prepared antiparallel order in vertical domain structures shown in Fig. 9. In separated samples, the thicknesses of adjacent layers

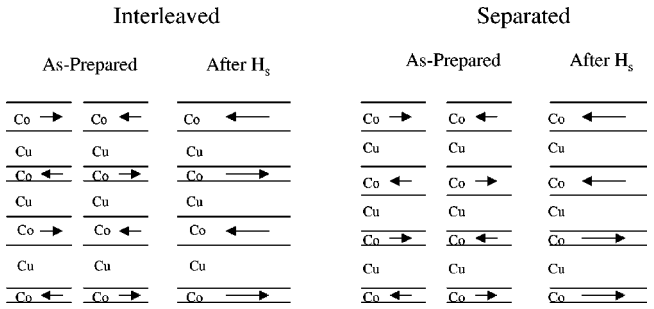

FIG. 9. Schematic, approximate pictures of inferred magnetic ordering for interleaved and separated samples in their ''as-prepared'' state and after they have been taken to saturation and then the field reversed only enough to flip the thicker Co layers.

are also all the same, except at the single boundary between thick and thin layers. In the as-prepared state, we, thus, expect almost as ideal AP domain structures as in simple $[F/N]_N$ multilayers. In interleaved samples, in contrast, adjacent layers always have different thicknesses. If the first layer is thick, its fringing fields will not be fully ''taken up'' by the second layer which is thinner, leaving some field lines to extend up to the third layer and compete against the smaller fringing fields from the second layer. This difference is compatible with a less ideal AP order of the as-prepared states of interleaved samples and the smaller values of $A\Delta R(0)$ in Figs. 1 and 2. Figure 9 shows the ideal pictures of the differences between as-prepared samples of interleaved and separated samples, and the same samples after being taken to H_s and then having the field reversed only enough to flip the thicker layers. In the as-prepared states, half of both thicker and thinner Co layers would already be oriented along any given field direction. Thus, as each different layer thickness flips, the changes in magnetizations should be only about half as large as when the same layers flip after the sample has been taken to saturation. These are the behaviors seen in Fig. 8.

3. Polarized neutron reflectivity results

PNR data generally support this picture of randomly oriented, micron-sized domains within the sample plane that become single domains in a saturating field. We examined an interleaved sample $[Co(6)/Cu(20)/Co(1)/Cu(20)]_8$ and a separated sample $[Co(6)/Cu(20)]_8[Co(1)/Cu(20)]_8$ with magnetoresistance and magnetization behaviors similar to those shown in Figs. 1 (bottom) and 7, respectively. After cooling in zero field and saturating in a field of -2000 Oe, we reversed the field and obtained the reflectivity of both samples in a field of 250 Oe (which coincides with the peak in the magnetoresistance of the interleaved sample), and in fields of 74, 114, and 725 Oe (the latter two of which are near the two peaks in the magnetoresistance of the separated sample). These results were compared to the reflectivity data measured in a saturating field $H_s > 1600$ Oe. The data obtained at all of these fields were characterized by the absence of specular spin-flip (SF) scattering. This result indicates that after saturation the Co moments are aligned either parallel or antiparallel to the applied field direction at all fields. Upon

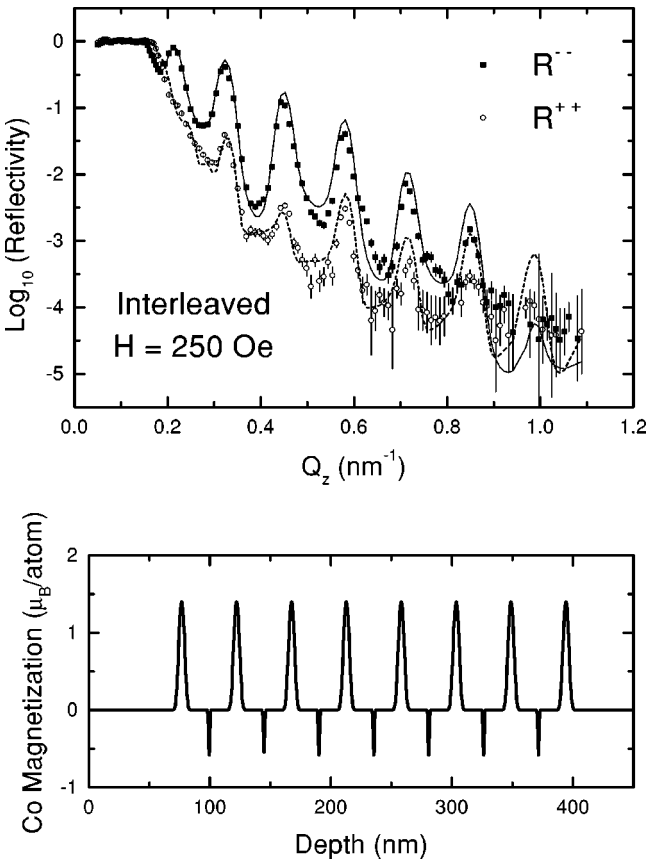

FIG. 10. Specular neutron reflectivity data and fits plotted as a function of the wave vector Q_z of an interleaved sample $[Co(6)/Cu(20)/Co(1)/Cu(20)]_8$ at 18 K in a 250 Oe field. Only the R^{--} (dark squares) and R^{++} (open circles) reflectivities are shown. (The SF reflectivities are effectively at the background level.) The magnetization profile for the Co layers that is shown in the bottom graph was obtained from the fit. The apparent differences in moments in the thin and thick layers are explained in the text.

field cycling, the reversal of the Co moment directions for the thick and thin layers thus occurs via domain formation, rather than moment rotation within the sample plane.

Figures 10 and 11 show the NSF specular reflectivity data and corresponding fits for the interleaved and separated samples, respectively, in a field of 250 Oe. In Fig. 10 the data for the interleaved sample are dominated by superlattice peaks above the critical angle at $Q = 0.21$, 0.32, 0.44, 0.58, 0.71, 0.85 nm$^{-1} \approx 2\pi m/D$, where $D = 45.4$ nm is the multilayer repeat length and m is an integer. (Note that this approximation does not explicitly hold for the peaks at low Q due to dynamical effects.) In contrast, the R^{--} data for the separated sample in Fig. 11 show superlattice peaks at $Q = 0.29, 0.52, 0.76$ nm$^{-1} \approx 2\pi m/D_1$, where $D_1 = 24.6$ nm, and the R^{++} data have superlattice peaks at $Q = 0.35$, 0.64, 0.95 nm$^{-1} \approx 2\pi m/D_2$, where $D_2 = 19.6$ nm. D_1 and D_2 correspond to the repeat lengths of the thick- and thin-layer parts of the multilayers, respectively, within the separated sample. The superlattice peaks for each multilayer appear in different reflectivity cross sections because the thin Co layers are aligned opposite to the 250 Oe field while the moments in

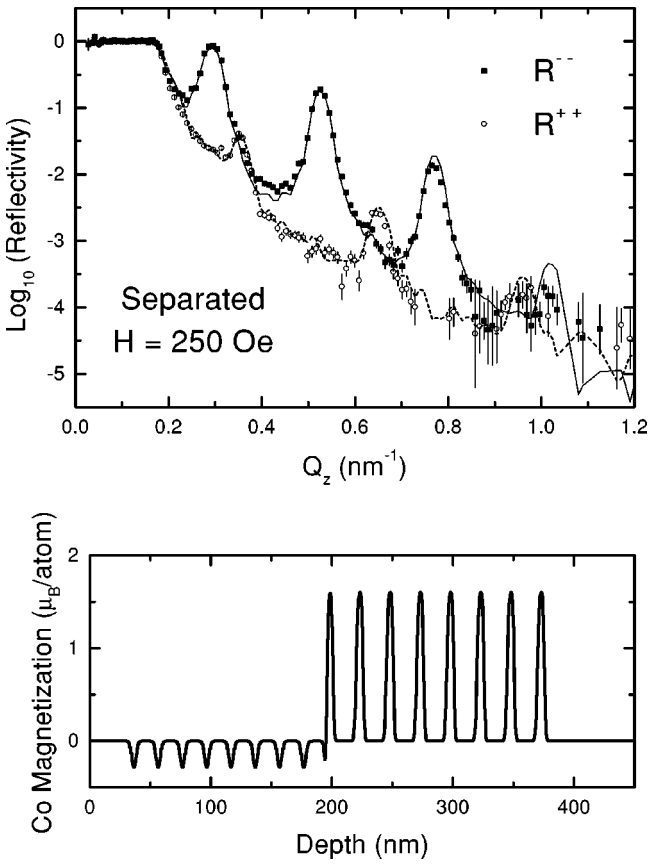

FIG. 11. Specular neutron reflectivity data and fits plotted as a function of the wave vector Q_z of a separated sample $[\mathrm{Co}(6)/\mathrm{Cu}(20)]_8[\mathrm{Co}(1)/\mathrm{Cu}(20)]_8$ at 18 K in a 250 Oe field. Only the R^{--} (dark squares) and R^{++} (open circles) reflectivities are shown. (The SF reflectivities are effectively at the background level.) The magnetization profile for the Co layers that is shown in the bottom graph was obtained from the fit. The apparent differences in moments in the thin and thick layers are explained in the text.

the thick Co layers are aligned parallel to the field. (In a saturating field, both sets of superlattice peaks are evident only in the R^{--} data.) In general, the relative intensities of the superlattice peaks in the R^{++} and R^{--} data are sensitive to the magnitude and orientation of the moments in the thin and thick Co layers averaged across the sample plane. The magnetization profiles at the bottom of Figs. 10 and 11 were generated from the fits to the corresponding PNR data. Consistent with the magnetization results (Fig. 7), our fits reveal that the Co moments in the thin and thick layers are aligned AP to each other for both samples at 250 Oe, as represented schematically in Fig. 9 (''after H_s''). The apparent moments in the thin Co layers, however, appear to be substantially smaller than those in the thick Co layers. This illusion occurs primarily because the fits are sensitive to the structural interfacial roughness averaged across the sample plane, which exceeds the 1 nm thickness of the thin layers along the growth direction. In reality, the moments in both the thick and thin layers saturate in a field of 2000 Oe to almost 100% of the bulk Co value. In a field of 250 Oe (Figs. 10 and 11), the magnetizations of the thin Co layers in both samples are only slightly reduced from their 2000 Oe saturation values, suggesting that small in-plane domains form within these layers as the field is raised toward its coercive value.

Specular reflectivity data at 73, 114, and 725 Oe confirm that the thin and thick Co layer moments reverse directions, as expected, at different coercive fields. After saturation in -2000 Oe. the moments in the thick Co layers in both the interleaved and separated samples start to reverse as the field passes zero, reach a net value of $M \sim 0$ at about 100 Oe, and are fully reversed by 250 Oe. The behavior around 100 Oe is evidenced, in part, by a large reduction of the fitted moments for the thick Co layers compared to their saturation value, as well as by an increase in the diffuse scattering.[18] As stated previously, this moment reversal occurs via the formation of small, in-plane domains. Over this field range, the moments in the thin Co layers remain parallel to the original field direction. Those moments begin to reorient as the field rises above 300 Oe, reaching $M \sim 0$ at about 725 Oe, and do not fully reverse until above 1000 Oe. Fits to the 725 Oe reflectivity data for both the interleaved and separated samples indicate that the Co moments in the thin layers, averaged across the sample plane, are reduced from their saturation value. The data thus suggest that the reversal of the thin Co layer moments also proceeds via formation of small, in-plane domains. The reflectivity data thus confirm that the peak/plateau in the magnetoresistance of interleaved/separated sample near 250 Oe (Figs. 1 and 2) is associated with an antiparallel alignment of the moments in the thin Co layers relative to those in the thick Co layers. In contrast, the peaks in magnetoresistance of the separated sample near 100 and 725 Oe (Figs. 1 and 2) are associated with the process of reversal of the thick (100 Oe) or thin (725 Oe) Co layers, respectively—i.e., with fully aligned thin Co layers at 100 Oe and thick Co layers at 725 Oe, but with the net magnetizations close to zero for the thick layers at 100 Oe or thin layers at 725 Oe. The orientation and magnitude of the thin and thick Co layer moments thus have a similar field dependence for both the interleaved and separated samples. Any unanticipated differences in magnetic structures between interleaved or separated samples in their nominal AP or P states appear too small to explain the differences between the magnetoresistances in Figs. 1 and 2.

The PNR data also provide information about the magnetic structures of the samples in their as-prepared states. Figure 12 shows the specular and diffuse reflectivity data for the separated sample. The R^{++} and R^{--} data show structural superlattice peaks at $Q = 2\pi m/D_1 = 0.29$, 0.52, 0.76 nm^{-1} from the thick-layer part of the multilayer ($D_1 = 24.6$ nm) and peaks at $Q = 2\pi m/D_2 = 0.35$, 0.64, 0.95 nm^{-1} ($D_2 = 19.6$ nm) from the thin-layer part of the multilayer. Unlike the data of Fig. 11, the NSF reflectivities are not split and provide no direct information about the magnetic structure. However, the magnetic SF data show broad features near these same positions indicating that some fraction of the sample with in-plane domain sizes larger than 100 μm is ordered with moments in the thick Co layers aligned antiparallel to those in the thin Co layers. This is comparable to the magnetic structure shown in the bottom

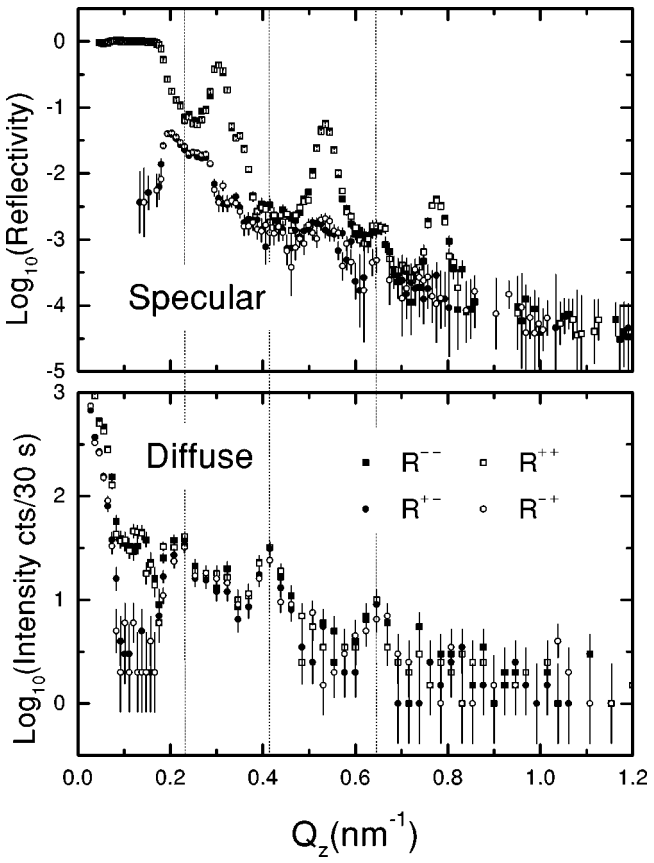

FIG. 12. Specular and diffuse reflectivity data for the separated sample $[\mathrm{Co}(6)/\mathrm{Cu}(20)]_8[\mathrm{Co}(1)/\mathrm{Cu}(20)]_8$ at 18 K in the as-prepared state. The data were obtained in a 3 Oe guide field. The R^{--} (dark squares), R^{++} (open squares), R^{+-} (dark circles), and R^{-+} (open circles) reflectivities are all shown. The diffuse data have not been corrected for polarization efficiencies. The vertical dotted lines mark the superlattice peaks in the diffuse data.

half of Fig. 11. The as-prepared data also show substantial magnetic diffuse scattering (bottom part of Fig. 12) indicating that a different portion of the sample orders with in-plane ferromagnetic domains sizes smaller than 100 μm.[17,18] Distinct peaks are apparent at $Q=0.22,0.42,0.65$ nm^{-1}. These magnetic peaks lie halfway between the structural superlattice peaks in the NSF data at $Q=2\pi m/D_1$. The periodicity of this magnetic structure is thus double the periodicity of the thick part of the separated multilayer. The presence of these peaks indicates that some portions of the thick Co layers are magnetically ordered in small, ferromagnetic in-plane domains that are oriented antiparallel relative to each other, as depicted in Fig. 9 (''as-prepared''). The in-plane direction of these domains is apparently random since the magnetic intensity is evenly distributed in the NSF and SF diffuse reflectivities. Unfortunately, neither the diffuse nor specular data provide any direct information about the magnetic ordering of the thin-layer part of the separated multilayers. While the as-prepared magnetic structure is clearly a mixture of several spin configurations, we can conclude that the sample partially orders in the antiparallel structure shown in Fig. 9 (''as-prepared'').

B. Magnetoresistance

If t/λ is the controlling parameter in the differences between interleaved and separated samples in Fig. 1, then greatly increasing it in either the F or N metal should cause the data for separated samples to approach those for interleaved ones, provided that l_{sf} remains long enough. To test this expectation we replaced Cu by Cu(2%Ge) hereafter just CuGe, which has short $\lambda_{\mathrm{CuGe}}\sim 8$ nm,[13,16] but long $l_{\mathrm{sf}}^{\mathrm{CuGe}}\sim 130$ nm.[13] For $t_{\mathrm{CuGe}}=20$ nm and 40 nm (Figs. 2, 3 and Ref. 13), the ratios $t_{\mathrm{CuGe}}/\lambda_{\mathrm{CuGe}}$ are 2.5 and 5. For $t_{\mathrm{CuGe}}=20$ nm and $N=2$ (Fig. 3), the ratio $t_T/l_{\mathrm{sf}}^{\mathrm{CuGe}}<1$, where $t_T=60$ nm is the total CuGe thickness between outer Co layers. For $t_{\mathrm{CuGe}}=10$ nm and $N=3$ (Ref. 13), $t_T/l_{\mathrm{sf}}^{\mathrm{CuGe}}<0.4$ is even smaller. Figure 4 and Ref. 14 showed further that the differences were not reduced by increasing the layer-thickness to mean-free-path ratios in all three layers by more than a factor of 10, by also replacing the 1 nm thick Co layers by 30 nm thick Py layers and the 6 nm thick Co layers by 15 or 30 nm thick CoZr layers.

From these results, we conclude that the ratio t/λ is not driving the differences between interleaved and separated data—there are no ''mean-free-path effects'' of the kind described in Ref. 10. We already noted in Sec. III that the differences in magnitudes of the data for Cu and CuGe inserts can be mostly explained by the different values of $AR(\mathrm{AP})$ [see Eqs. (1) and (2)]. Any residual differences can presumably be ascribed to effects of finite l_{sf} not included in Eqs. (1) and (2).

We next ask what contribution to the data of Figs. 1 and 2 can come from VF theory with finite bulk spin-diffusion lengths, l_{sf}, for Co, Cu, and CuGe. Published estimates of $l_{\mathrm{sf}}^{\mathrm{Co}}$ lie in the range 60 ± 20 nm.[27,29] For Cu, we estimated $l_{\mathrm{sf}}^{\mathrm{Cu}}\sim 500$ nm,[30] with uncertainty from 400 nm to 1 μm. For CuGe we estimated $l_{\mathrm{sf}}^{\mathrm{CuGe}}=130\pm 30$ nm from the data of Ref. 9. For quantitative comparison of separated (sep) and interleaved (int) samples, we examine the ratio $(A\Delta R)_{\mathrm{sep}}/(A\Delta R)_{\mathrm{int}}$. Experimentally, we take $(A\Delta R)_{\mathrm{int}}$ at the peak of the interleaved data, and $(A\Delta R)_{\mathrm{sep}}$ at the plateau just beyond the first peak of the separated data. The results for $t_{\mathrm{N}}=20$ nm are shown as a function of N in Fig. 13 for samples with both Cu and CuGe. The predictions of VF theory for this ratio, assuming $l_{\mathrm{sf}}^{\mathrm{Co}}=60$ nm, $l_{\mathrm{sf}}^{\mathrm{Cu}}=500$ nm, and $l_{\mathrm{sf}}^{\mathrm{CuGe}}=130$ nm are the dotted and long-dashed curves, with error bars showing the ranges of uncertainties due to the uncertainties in l_{sf} listed above. These two curves account for 20 to 50 % of the observed differences between interleaved and separated samples. We, thus, disagree with Ref. 10 that finite values of l_{sf} are irrelevant to the differences in Fig. 1, but we agree that a further mechanism is needed to fully explain those differences. To account for them by $l_{\mathrm{sf}}^{\mathrm{Co}}$ alone would require $l_{\mathrm{sf}}^{\mathrm{Co}}\sim 10$ nm, a value that seems too short.

An intriguing possibility is spin-memory loss (spin flipping) at F/N interfaces.[12,13,25] With no direct evidence for such loss, our analysis must be indirect. We showed in Sec. III C that modest spin-memory loss at F/N interfaces would not destroy the agreement of published data with 2CSR and VF models. We also recently showed that spin-memory loss can be large at N1/N2 interfaces; values for V/Cu, Nb/Cu,

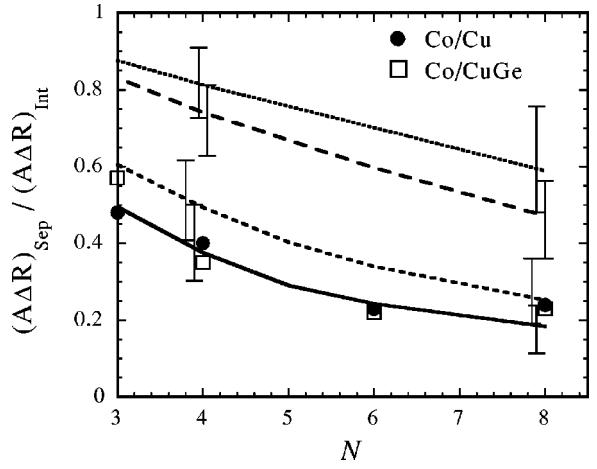

FIG. 13. $(A\Delta R)_{sep}/(A\Delta R)_{int}$ vs N. The dotted and long-dashed curves for Co/Cu and Co/CuGe, respectively, are predictions using VF theory with the parameters for Co/Cu (Ref. 27) plus $l_{sf}^{Co}=60$ nm, $l_{sf}^{Cu}=500$ nm, and $l_{sf}^{CuGe}=130$ nm. The vertical bars indicate the ranges of uncertainties due to uncertainties in these values of l_{sf}. The short-dashed curve for Co/Cu and the solid curve for Co/CuGe add $\delta_I=0.25$ to the prior calculations. Now the error bars indicate the ranges of predictions for $\delta_I=0.25\pm0.1$. For these curves, the error bars due to uncertainties in l_{sf} are smaller than the symbols for the data.

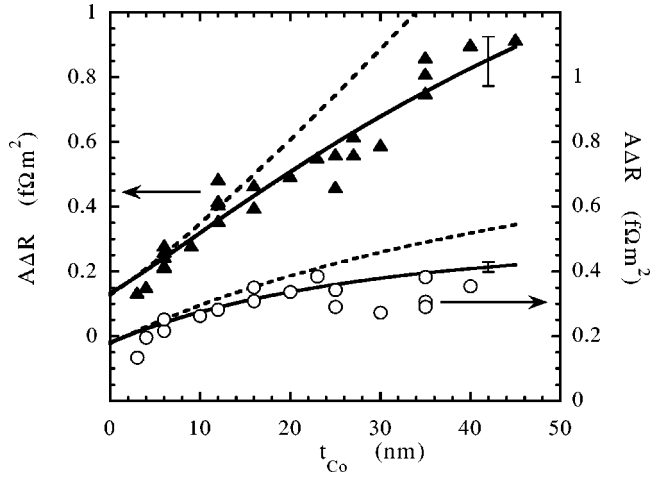

FIG. 14. $A\Delta R$ vs t_{Co} for symmetric (filled triangles) and asymmetric (open circles) Co/Cu exchange-biased spin valves. The dashed curves are prior fits (Ref. 27) assuming no spin-memory loss at the Co/Cu interfaces. The solid curves just add an interfacial spin-memory loss of $\delta_I=0.25$.

and W/Cu ranged from ~6%/interface for V/Cu up to ~60%/interface for W/Cu.[26] We attributed these losses to spin-orbit-induced spin flipping in high-resistivity interfacial alloys. Adding additional flipping due to magnetic disorder in alloyed regions at F/N interfaces could well enhance interfacial spin-memory loss.

The short-dashed curve for Co/Cu and the solid curve for Co/CuGe in Fig. 13 show our calculations of $(A\Delta R)_{sep}/(A\Delta R)_{int}$ adding $\delta_I=0.25$ to the spin-diffusion lengths listed above. The uncertainties in these curves due to those in l_{sf} are no larger than the sizes of the symbols for the data. The uncertainty bars shown for these curves are for $\delta_I=0.25\pm0.1$. We conclude this discussion of spin-memory loss at Co/Cu interfaces by (a) arguing that the loss observed is plausible if the interface is viewed as a random alloy of Co and Cu and (b) showing that some previously published data provide indirect support for such loss.

(a) We estimate $\delta_I=t_I/l_{sf}^I$ for an assumed Co-Cu 50-50 alloy with thickness t_I assuming that spin-flips are due to spin-orbit scattering. Since the spin-orbit cross section of Co in Cu is rather uncertain,[31] and we do not have reliable information about the "size-effect" parameter $\rho_I\lambda_I$ (Ref. 15) for the interfacial alloy, we must make assumptions. We assume that $\rho_I\lambda_I$ has the typical value[15] $\rho_I\lambda_I=1$ fΩm^2, and that $\rho_I t_I=AR^*_{Co/Cu}(1-\gamma^2)$, where $AR^*_{Co/Cu}=0.5$ fΩm^2 is the measured Co/Cu interfacial resistance.[6] Dividing the second relation by the first, we find $t_I/\lambda_I\approx0.2$. To calculate δ_I, we must relate λ_I to l_{sf}^I. To do so, we assume that the minority and majority mean-free paths in the interface have the ratio set by our measured γ for Co/Cu interfaces—i.e., that $\lambda_I^\uparrow$ and $\lambda_I^\downarrow$ are related by $\lambda_I^\uparrow/\lambda_I^\downarrow=AR^\downarrow_{Co/Cu}/AR^\uparrow_{Co/Cu}=(1+\gamma)/(1-\gamma)\approx7$ (Ref. 6). Since the transport mean-free path is the sum of the spin-dependent mean-free paths, the effective mean-free path related to the interface resistivity ρ_I is essentially just the long one $\lambda_I^\uparrow$. From Eq. (10) of Fert *et al.*,[32] l_{sf}^I is related to the mean-free path for spin-orbit scattering λ_{sf} by the expression $l_{sf}^I=\sqrt{[\lambda_I^\downarrow\lambda_I^\uparrow\lambda_{sf}]/[3(\lambda_I^\downarrow+\lambda_I^\uparrow)]}$. Since $\lambda_I^\uparrow\gg\lambda_I^\downarrow$, one obtains $l_{sf}^I\approx\sqrt{(\lambda_I^\downarrow\lambda_{sf})/3}$. If, from Ref. 31, we take $\lambda_{sf}\sim20\lambda_I^\uparrow$ (20 times the transport mean-free path), we obtain $l_{sf}^I\approx\lambda_I^\uparrow\sqrt{20/(7\times3)}\approx\lambda_I^\uparrow$. Our estimate then becomes $\delta_I=t_I/l_{sf}^I=t_I/\lambda_I^\uparrow=0.2$, large enough to "justify" our experimental estimate of $\delta_I\approx0.25$.

(b) As noted in Sec. III C, adding an interfacial $\delta_I=0.25$ has minimal effect on $A\Delta R$ for simple F/N multilayers with identical F layers, or for interleaved multilayers. Such an addition can, however, affect $A\Delta R$ in exchange-biased spin valves (SV's). In an earlier paper[27] we reported that data for both symmetric (equal Co layer thicknesses) and asymmetric (one Co layer thickness fixed and one variable) Co/Cu exchange-biased SV's fell below the values predicted using nonadjustable, independently determined, CPP-MR parameters for Co, Cu, and Co/Cu interfaces. Figure 14 shows those data and those fits (dashed curves). We also noted[27] that most of the discrepancies could be removed by a combination of modest variations in the assumed parameters plus corrections for failure to reach a fully AP state in the symmetric SVs with thick Co layers. The solid curves in Fig. 14 show that an interfacial spin-memory loss of $\delta_I=0.25$ provides an alternative possible explanation. These curves (and the uncertainty bars shown) were calculated using exactly the same parameters as for the dashed curves, but simply adding interfacial spin-memory loss of $\delta_I=0.25\pm0.1$. This completely nonadjustable procedure fits both sets of data surprisingly well.

For completeness, we also consider measurements of the CIP MR's of interleaved and separated Co/Cu multilayers. If mean-free paths were the dominant length scales in both the CIP and CPP MR's, the two might be expected to show

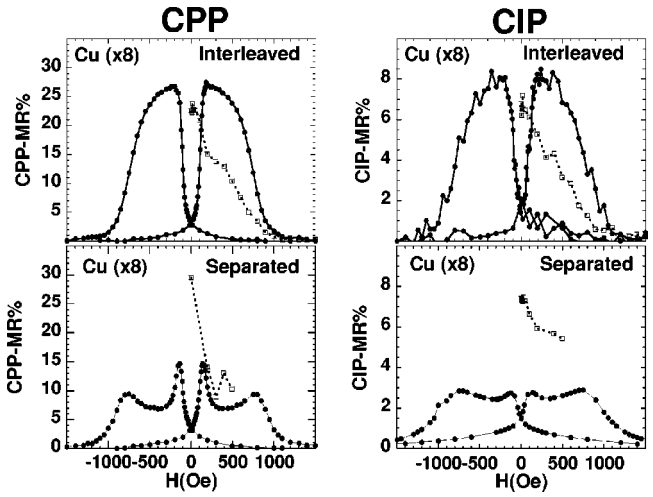

FIG. 15. Comparison of CPP MR and CIP MR for separated and interleaved Co/Cu multilayers. Symbols and curves have the same meanings as in Fig. 1. The open squares for the separated CPP-MR were noisy, as shown by the fluctuations in the points for $H=200$ -500 Oe. To reduce uncertainty at $H\approx 0$, that square is the average of six very low field measurements. All other points are single measurements.

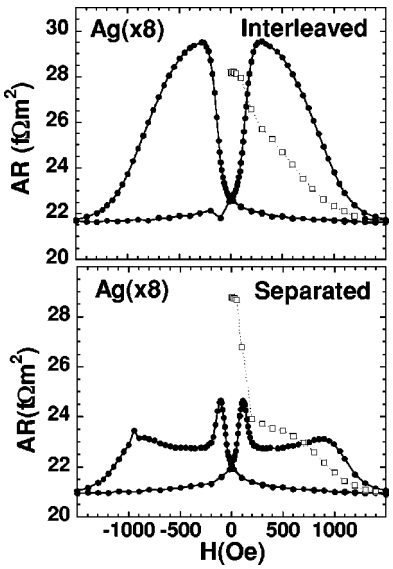

FIG. 16. $AR(H)$ vs H at 4.2 K for interleaved (top) and separated (bottom) multilayers of Co/Ag with $N=8$. The scale units for this pair of samples are identical. The open squares and dashed curves show how $AR(H)$ varied when first taken from the as-prepared state to the saturated state. The filled circles and solid curves show how it varied after having been taken to saturation.

similar differences between interleaved and separated samples. Indeed, we previously reported similar differences for [Py/Ag/Co/Ag] multilayers,[11] but attributed them to different underlying physics, mean-free-path limitations for CIP, as noted in the Introduction above, and spin-diffusion length limitations, mostly in the Py, for CPP. Figure 15 shows that we find similar differences in the CIP MR's and CPP MR's for Co/Cu multilayers. Again, we attribute them to different physics—the CIP MR's to expected mean-free-path effects there, and now the CPP MR's to a combination of spin-memory loss in the bulk materials and at the interfaces as argued above and in Refs. 13 and 14.

Lastly, to see if the results of Fig. 1 are highly sensitive to details of the mutual solubilities and band structures of the F and N metals, we checked the differences between interleaved and separated samples with Cu replaced by Ag, which is insoluble in Co. Figure 16 shows data similar to those in Fig. 1.

V. SUMMARY AND CONCLUSIONS

In this paper we have done the following.

(1) Confirmed the differences in CPP MR reported in Ref. 10 for interleaved $[\mathrm{Co}(6)/\mathrm{Cu}(20)/\mathrm{Co}(1)/\mathrm{Cu}(20)]_N$ and separated $[\mathrm{Co}(6)/\mathrm{Cu}(20)]_N[\mathrm{Co}(1)/\mathrm{Cu}(20)]_N$ multilayers after they are taken to above their saturation fields, and showed that the differences persist in samples with repeat numbers as small as $N=2$.

(2) Showed that the differences in CPP MR remain essentially unchanged when Cu is replaced by Cu(2%Ge) with thicknesses that increase the ratio $t_{\mathrm{Cu}}/\lambda_{\mathrm{Cu}}$ of mean-free path to layer thickness in the Cu from about 1/5 to 5, while still leaving the spin-diffusion length long. We infer that mean-free paths are not scaling lengths in the CPP MR of present day samples.

(3) Showed that the differences remain unchanged, or even increase, when the Co layers are replaced by Py and CoZr layers for which t/λ increases by more than factors of 10. This result is further evidence that the CPP-MR scaling lengths are spin-diffusion lengths, not mean-free paths.

(4) Used both magnetization and polarized neutron reflectivity measurements to show that (a) our samples do reach closely antiparallel (AP) states and at the same fields for both interleaved and separated samples and (b) any unwanted differences between the magnetic structures of interleaved and separated samples are small.

(5) Showed that the CPP MR's in the as-prepared states of separated samples are as large as those at the peaks of interleaved samples. We attribute this result to magnetic structures of the separated samples in the as-prepared state in which magnetizations of adjacent layers are reversed, as distinct from the state where the magnetizations of thick and thin layers are reversed. This result confirms the argument in Ref. 10 that the magnetic order of adjacent layers in separated samples is crucial. We showed that the specific model associated with that claim is essentially equivalent to Eq. (3) above, which extends VF theory to include interfacial spin flips. We dispute the claim[10] that such a model is "nonlocal," arguing that it is the most local model that gives a CPP MR.

(6) Confirmed the claim[10] that the best available spin-diffusion lengths in Co and Cu are too long to fully explain the observed differences in CPP MR between interleaved and separated samples, but showed that these lengths are short enough to account for part of those differences.

(7) Argued that the rest of the differences can plausibly be attributed to spin flipping at Co/Cu interfaces with spin-flipping parameter $\delta_I=0.25$, and showed that the same amount of flipping: (a) can resolve discrepancies between

predictions and previously obtained data on Co-Cu exchange-biased spin valves and (b) is consistent with a simple estimate of effects of spin-orbit scattering in an interfacial layer composed of a Co-Cu alloy.

(8) Showed that the differences between interleaved and separated states are similar in the CIP and CPP MR's, although we interpreted the two cases differently.

(9) Showed that similar differences between interleaved and separated states persist when the Cu is replaced by Ag, which we take as evidence that the differences between separated and interleaved samples are not sensitively dependent on details of mutual solubility or band structures.

We conclude that the observation[10] of differences in CPP MR between interleaved and separated samples of Co and Cu has been highly stimulating. If future work confirms the importance of spin flipping at F/N interfaces, Ref. 10 must be given credit for having led the way to this possibility. If, on the other hand, spin flipping at interfaces is not the source of the differences, then this source remains unclear, although mean-free-path effects seem ruled out. The use of the 2CSR and VF models in most published work on the CPP MR still seems justified, although if interfacial spin flipping at F/N interfaces is eventually confirmed, some parameters may need to be slightly modified.

ACKNOWLEDGMENTS

This work was supported by the MSU CFMR, CSM, U.S. NSF Grants No. DMR 98-20135 and 98-09688, and Seagate Technology.

[1] S.F. Lee, W.P. Pratt, Jr., Q. Yang, P. Holody, R. Loloee, P.A. Schroeder, and J. Bass, J. Magn. Magn. Mater. **118**, L1 (1993).
[2] P. M. Levy, *Solid State Physics*, edited by H. Ehrenreich and D. Turnbull (Academic Press, New York, 1994), Vol. 47, p. 367.
[3] M.A.M. Gijs and G.E.W. Bauer, Adv. Phys. **46**, 285 (1997).
[4] S. Zhang and P.M. Levy, J. Appl. Phys. **69**, 4786 (1991).
[5] T. Valet and A. Fert, Phys. Rev. B **48**, 7099 (1993).
[6] J. Bass and W.P. Pratt, Jr., J. Magn. J. Magn. Magn. Mater. **200**, 274 (1999).
[7] S.F. Lee, Q. Yang, P. Holody, R. Loloee, J.H. Hetherington, S. Mahmood, B. Ikegami, K. Vigen, L.L. Henry, P.A. Schroeder, W.P. Pratt, Jr., and J. Bass, Phys. Rev. B **52**, 15 426 (1995).
[8] A. Fert and L. Piraux, J. Magn. Magn. Mater. **200**, 338 (1999).
[9] J. Bass, P.A. Schroeder, W.P. Pratt, Jr., S.F. Lee, Q. Yang, P. Holody, L.L. Henry, and R. Loloee, Mater. Sci. Eng., B **31**, 77 (1995).
[10] D. Bozec, M.A. Howson, B.J. Hickey, S. Shatz, N. Wiser, E.Y. Tsymbal, and D.G. Pettifor, Phys. Rev. Lett. **85**, 1314 (2000); D. Bozec, M.J. Walker, M.A. Howson, B.J. Hickey, S. Shatz, and N. Wiser, J. Phys.: Condens. Matter **12**, 4263 (2000).
[11] W.-C. Chiang, Q. Yang, W.P. Pratt, Jr., R. Loloee, and J. Bass, J. Appl. Phys. **81**, 4570 (1997).
[12] D. Bozec, M.J. Walker, B.J. Hickey, M.A. Howson, and N. Wiser, Phys. Rev. B **60**, 3037 (1999).
[13] K. Eid, D. Portner, R. Loloee, W.P. Pratt, Jr., and J. Bass, J. Magn. Magn. Mater. **224**, L205 (2001).
[14] K. Eid, M. Tsoi, D. Portner, R. Loloee, W. P. Pratt, Jr., and J. Bass, J. Magn. Magn. Mat. (to be published).
[15] J. Bass, in *Metals, Electronic Transport Phenomena*, edited by K. H. Hellwege and J. L. Olson, Landolt-Bornstein, New Series, Group 3, Vol. 15 (Springer-Verlag, Berlin, 1982).
[16] C.F. Majkrzak, Physica B **221**, 342 (1996).
[17] S. K. Sinha, in *Neutron Scattering in Materials Science II*, edited by D. A. Neumann, T. P. Russell, and B. J. Wuensch, MRS Symp. Proc. No. 376 (Materials Research Society, Pittsburgh, 1995), p. 175.
[18] J.A. Borchers, J. Dura, J. Unguris, D. Tulchinsky, M.H. Kelley, C.F. Majkrzak, S.Y. Hsu, R. Loloee, W.P. Pratt, Jr., and J. Bass, Phys. Rev. Lett. **82**, 2796 (1999); J.A. Borchers, J.A. Dura, C.F. Majkrzak, S.Y. Hsu, R. Loloee, W.P. Pratt, Jr., and J. Bass, Physica B **283**, 162 (2000).
[19] J.A. Borchers, P.M. Gehring, R.W. Erwin, J.F. Ankner, C.F. Majkrzak, T.L. Hylton, K.R. Coffey, M.A. Parker, and J.K. Howard, Phys. Rev. B **54**, 9870 (1996).
[20] K.M. Schep, J.B.A.N. van Hoof, P.J. Kelley, G.E.W. Bauer, and J.E. Inglesfield, Phys. Rev. B **56**, 10 805 (1997).
[21] K. Xia, P.J. Kelly, G.E.W. Bauer, I. Turek, J. Kudrnovsky, and V. Drchal, Phys. Rev. B **63**, 064407 (2001).
[22] E. Tsymbal and D. G. Pettifor, in *Solid State Physics*, edited by H. Ehrenreich and F. Spaepen (Academic Press, New York, 2001), Vol. 56, p. 113.
[23] S.D. Steenwyk, S.Y. Hsu, R. Loloee, J. Bass, and W.P. Pratt, Jr., J. Magn. Magn. Mater. **170**, L1 (1997).
[24] K. Eid (unpublished).
[25] A. Fert and S.F. Lee, Phys. Rev. B **53**, 6554 (1996).
[26] W. Park, D.V. Baxter, S. Steenwyk, I. Moraru, W.P. Pratt, Jr., and J. Bass, Phys. Rev. B **62**, 1178 (2000).
[27] A. Reilly, W.-C. Chiang, W. Park, S.Y. Hsu, R. Loloee, S. Steenwyk, W.P. Pratt, Jr., and J. Bass, IEEE Trans. Magn. **34**, 939 (1998).
[28] J.Y. Gu, S.D. Steenwyk, A.C. Reilly, W. Park, R. Loloee, J. Bass, and W.P. Pratt, Jr., J. Appl. Phys. **87**, 4831 (2000).
[29] L. Piraux, S. Dubois, A. Fert, and L. Belliard, Eur. Phys. J. B **4**, 413 (1998).
[30] Q. Yang, P. Holody, S.-F. Lee, L.L. Henry, R. Loloee, P.A. Schroeder, W.P. Pratt, Jr., and J. Bass, Phys. Rev. Lett. **72**, 3274 (1994).
[31] P. Monod and S. Schultz, J. Phys. (Paris) **43**, 393 (1982).
[32] A. Fert, J.L. Duvail, and T. Valet, Phys. Rev. B **52**, 6513 (1995).